Available online at www.sciencedirect.com
SCIENCE DIRECT®
Journal of Nuclear Materials 352 (2006) 62–74
journal of nuclear materials
www.elsevier.com/locate/jnucmat

# Three dimensional observations and modelling of intergranular stress corrosion cracking in austenitic stainless steel

T.J. Marrow [a,*], L. Babout [a], A.P. Jivkov [a], P. Wood [a], D. Engelberg [a], N. Stevens [a], P.J. Withers [a], R.C. Newman [b]

[a] *Materials Performance Centre, School of Materials, University of Manchester, P.O. Box 88, M1 7HS, UK*
[b] *Department of Chemical Engineering and Applied Chemistry, University of Toronto, Canada*

**Abstract**

Stress corrosion cracking is a life-limiting factor in many components of nuclear power plant in which failure of structural components presents a substantial hazard to both safety and economic performance. Uncertainties in the kinetics of short crack behaviour can have a strong influence on lifetime prediction, and arise due both to the complexity of the underlying mechanisms and to the difficulties of making experimental observations. This paper reports on an on-going research programme into the dynamics and morphology of intergranular stress corrosion cracking in austenitic stainless steels in simulated light water environments, which makes use of recent advances in high resolution X-ray microtomography. In particular in situ, three dimensional X-ray tomographic images of intergranular stress corrosion crack nucleation and growth in sensitised austenitic stainless steel provide evidence for the development of crack bridging ligaments, caused by the resistance of non-sensitised special grain boundaries. In parallel a simple grain bridging model, introduced to quantify the effect of crack bridging on crack development, has been assessed for thermo-mechanically processed microstructures via statically loaded room temperature simulant solution tests and as well as high temperature/pressure autoclave studies. Thermo-mechanical treatments have been used to modify the grain size, grain boundary character and triple junction distributions, with a consequent effect on crack behaviour. Preliminary three-dimensional finite element models of intergranular crack propagation have been developed, with the aim of investigating the development of crack bridging and its effects on crack propagation and crack coalescence.


*PACS:* 62.20.Mk; 81.70.Tx; 02.70.Dc

## 1. Introduction

Stress corrosion cracking is a significant potential cause of failures in the nuclear power industry [1]. Cracking frequently nucleates from corrosion pits [2] and, depending on the material and environment,

* Corresponding author. Tel.: +44 (0) 161 306 3611; fax: +44 (0) 161 306 3586.
*E-mail address:* james.marrow@manchester.ac.uk (T.J. Marrow).

0022-3115/$ - see front matter © 2006 Elsevier B.V. All rights reserved.
doi:10.1016/j.jnucmat.2006.02.042

may be transgranular or intergranular in nature. The incubation period prior to the development of a critical crack nucleus depends on several factors [3]. These include the rate of pit/localized corrosion formation and growth, the transition from pit/localized corrosion to crack initiation, and the propagation of short cracks with a size comparable to the microstructure scale. Although models for these processes have been developed [3,4], the prediction of incubation periods remains uncertain due to the complex interaction between microstructure, environment and the mechanisms of localized corrosion and environmentally assisted cracking.

Resistance to intergranular corrosion and stress corrosion cracking can be affected by the distribution of grain boundary crystallographic character [5]. In particular, the grain boundary character may affect intergranular failure via its effect on solute concentrations [6] and precipitation [7]. Grain boundary engineering provides a means to improve the resistance to intergranular stress corrosion cracking by disrupting easy pathways through the microstructure [8]. The interactions between the crack and the microstructure are expected to be most significant when the crack is a short crack. However, very little is known about the behaviour of short stress corrosion cracks due to experimental difficulties in monitoring their nucleation and growth.

This paper describes how in situ three-dimensional observations of the evolution of intergranular stress corrosion cracking in sensitised stainless steel have provided evidence for a crack bridging mechanism, by which the resistance to propagation of short stress corrosion cracks can be influenced by the grain boundary triple junction distribution. Experimental data for the effect of microstructure engineering on crack propagation resistance, and a comparison between the crack propagation in different environments is also presented. These observations provide the mechanistic basis for a new three-dimensional computational model of short stress corrosion crack propagation, which will enable crack coalescence behaviour and the role of residual stress gradients to be investigated.

## 2. Experimental methods

### 2.1. Tomographic imaging of SCC In 302 stainless steel

In order to investigate the interaction between a propagating crack and the microstructure in situ three dimensional observations of intergranular stress corrosion cracking were performed, using the ID19 X-ray microtomography beam line at the European Synchrotron Radiation Facility (ESRF), France. An annealed and fully sensitised 302 stainless steel wire (400 μm diameter) (Table 1) was tested in 0.15 M potassium tetrathionate ($K_2S_4O_6$) (pH 2). Tetrathionate solutions [9], are known to attack chromium depleted zones [10]. The degree of intergranular corrosion is therefore determined by the degree of chromium depletion, which is affected by the grain boundary character (CSL) and the sensitisation treatment [11].

Details of the synchrotron tomography technique [12,13] and the experimental set-up employed here [14,15] are described elsewhere. In essence, the wire was spot-welded to 3 mm diameter steel grub screws to form a tensile specimen, which was then lacquered to expose a gauge length of approximately 0.5 mm. The specimen was tested under load (up to 200 MPa) in an environmental cell on the ID19 stage (Fig. 1). Cracking was initiated by coupling the sample to a platinum working electrode for a few seconds to polarize the stainless steel wire anodically. Preliminary experiments demonstrated that cracking would then occur under open circuit conditions, and could be suspended for tomographic imaging by simultaneously reducing the load and coupling the stainless steel wire to a pure aluminium electrode to impose a cathodic polarisation. Cracking re-initiated when open circuit conditions were restored. Cracking occurred rapidly on re-application of the stress, which was progressively reduced as cracking was observed. The initiation of cracking and subsequent specimen failure due to coalescence was recorded in samples sensitised for 1 h at 923 K (650 °C). X-ray imaging was undertaken at an energy of 30 keV. Thousand radiographs were taken

Table 1
Chemical composition (wt%)

| UNS | Fe | Cr | Ni | C | Mn | P | S | Si | N |
|---|---|---|---|---|---|---|---|---|---|
| S30400 | Bal. | 18.15 | 8.60 | 0.055 | 1.38 | 0.032 | 0.005 | 0.45 | 0.038 |
| S30200 | Bal. | 18.14 | 8.60 | 0.070 | 1.25 | 0.025 | 0.003 | 0.40 | n.a. |

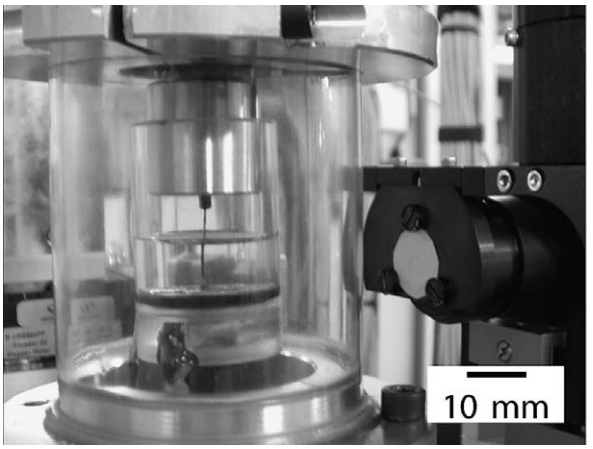


Fig. 1. Unloaded stainless steel wire sample in the environmental cell. The inner Perspex tube contains the 0.15 M potassium tetrathionate solution, the outer tube acts as the load column. Both are transparent to X-rays. The CCD imaging detector is to the right of the image.

in 90 min for each tomograph and were reconstructed by the back projection method. During the stress corrosion experiment, five tomographic images were acquired.

### 2.2. 304 Stainless test microstructures

To obtain characteristic microstructures to test predictive models, samples of type 304 austenitic stainless steel plate (Table 1) were thermo-mechanically processed, comprising unidirectional cold rolling to introduce 30% strain, followed by heat treatment in argon atmosphere at 1173 K (900 °C) for 30 min with a subsequent water quench (900/30). This was compared with the as-received microstructure. Full details of the experiments, and the results of processing a wider range of microstructures, are reported elsewhere [16]. The basic microstructural features were quantified by electron backscatter diffraction (EBSD) with an HKL-EBSD system, interfaced to a Philips XL-30 FEGSEM. Details of the data processing and analysis are reported elsewhere [17].

The information obtained by EBSD included the Grain Boundary Character (GBCD) and Triple Junction (TJD) distributions, using the Coincidence Site Lattice model (CSL) [18]. The low angle grain boundary (LAGB) threshold was set to 1.6°, with 15° for high angle grain boundaries (HAGB), by applying Brandon's criterion ($\Delta\theta = 15 \times \Sigma^{-1/2}$) [19] for the maximum allowed deviation angle. The microstructural parameters for the two microstructures are summarised in Table 2 where it can be seen that considerable microstructural refinement and a measured reduction in the percentage of Σ3 boundaries has been brought about by the (900/30) recrystallisation treatment.

### 2.3. Room temperature crack propagation tests

Crack propagation experiments were performed on the test microstructures to determine the effects of microstructure on crack propagation behaviour. Double-beam-bent specimens (DBB) (i.e. self-stressed four point bending) [20] were employed enabling us to investigate the extent of crack propagation as a function of applied static stress, test duration and microstructure. The sample size was approximately $200\ \text{mm} \times 20\ \text{mm} \times 41.5\ \text{mm}$. The test electrolyte was aqueous 0.1 M potassium tetrathionate solution, acidified with diluted sulphuric acid to pH 2.5. All samples were fully sensitised at 923 K (650 °C) for 24 h. After removal from the test environment and unloading, each specimen was strained in tension to open the intergranular cracks for observation. The cracks were found to lie within a log-normal population [16], and hence extreme value statistics, in the form of Gumbel distributions, were applied to evaluate the crack population [21,22]. This method allows the crack population to be described by measuring the longest crack in each sub-area of the sample.

### 2.4. High temperature crack propagation tests

High temperature stress corrosion crack propagation tests were conducted using the as-received

Table 2
Summary of microstructure parameters for grain boundary and triple junction distribution for the as-received microstructure and after a 30% strain, 1173 K (900 °C) anneal for 30 min (900/30)

| Structure | Grain size, $D$ (μm) (including twins) | Grain size, $D$ (μm) (excluding twins) | Fraction of low CSL boundaries ($\Sigma \leqslant 29$) (%) | Fraction of Σ3 boundaries (%) |
|---|---|---|---|---|
| As-rec | $20.6 \pm 3.1$ | $26.5 \pm 4.5$ | $35.2 \pm 3.2$ | $21.8 \pm 0.7$ |
| 900/30 | $9.5 \pm 0.2$ | $11.4 \pm 0.3$ | $27.2 \pm 0.8$ | $13.3 \pm 0.2$ |

304 stainless steel (Table 1) (fully sensitised at 923 K for 20 h) to demonstrate that the crack bridging mechanism was not unique to the tetrathionate environment. A Cormet Testing Systems 10 kN constant load autoclave comprising a manually operated constant load unit, internal palladium reference electrode and computer system was used with a 0.01 M $Na_2SO_4$ electrolyte at 523 K (250 °C) and a pressure of 40 bar. The tensile specimens, which had a gauge length of 20 mm and diameter 2.5 mm, were polarised to 500 mV above their rest potential under static load (90% of room temperature yield stress) to promote stress corrosion cracking.

## 3. 3D observations of intergranular stress corrosion cracking

The principal finding arising from this experiment was the demonstration of the formation and failure of crack bridging ligaments. Crack bridging is a common phenomenon in the brittle fracture of materials, such as from ceramics [23] to fiber-reinforced composites [24], whereby isolated regions of material link the opposing faces of a crack and restrict its opening. It has not been reported previously for stress corrosion cracking, to the authors' knowledge. For example, Fig. 2(a)–(c) presents a sequence of longitudinal slices from the reconstructed tomographs at three different stages of stress corrosion cracking of the test wire, each slice taken at approximately the same location (70 μm from the sample centre). Two stress corrosion crack tips visible in these slices (identified as cracks 1 and 2 in Fig. 2) have been studied. Discontinuity A corresponds to an arrested crack tip, while B and C are crack bridging ligaments which develop and then fail as the crack opening displacement increases. 3D isosurface rendering [25] of the tomographic data has been used to visualise the crack bridges in Fig. 2(d) and (e).

Fractography of the sample after testing shows ductile features (e.g. Fig. 3(a)), with geometries that indicate that they are defined by twin boundaries (Fig. 3(b)). The twin boundaries are not sensitised, which is evidenced by the lack of intergranular cracking along the interface. EBSD analysis of a wide range of thermo-mechanically processed microstructures, processed with 30% strain and annealed at temperatures between 1173 and 1373 K (900 and 1100 °C) for times between 2 min and 24 h [16], show a high number of 2-CSL triple junctions where a low CSL boundary ($\leqslant\Sigma29$, $\neq\Sigma3$) is connected to a Σ3 twin boundary. Data for the effect of grain size (determined by the line intercept method, excluding Σ3 twin boundaries) on the average length of Σ3 twin and connected low CSL ($\leqslant\Sigma29$, $\neq\Sigma3$) boundaries is given in Fig. 4(a), with the as-received and 900/30 microstructures identified.

The connected low CSL length is proportional to the twin length, which is shown to be equivalent to the grain size. It is postulated that the observed ductile regions correspond to an area defined by a non-sensitised low CSL boundary, which associated with the growth of the twin during recrystallisation (Fig. 3(b)). The data in Fig. 4(a) indicate that the average area of such a region is proportional to the average grain boundary area (i.e. the square of grain size). The tensile failure of these ductile features implies that they have the potential to shield the crack tip from the applied stress. High resolution electron backscatter diffraction (EBSD) of sectioned crack paths (Fig. 4(b)) also suggests that such crack bridges can result from the intersection of the crack with twin-related features.

These observations indicate that *microstructural engineering* [5–8], which aims to increase resistance to intergranular stress corrosion crack propagation by increasing the number of twin-related non-sensitised grain boundary segments factors in the microstructure, will also increase the number of features with the potential to form ductile crack bridging ligaments. It is proposed that these ligaments are a significant factor in increasing the resistance of the microstructure to stress corrosion cracking.

## 4. Microstructural effects on SCC resistance

A microstructure engineering study was performed to investigate the effects of thermo-mechanical processing on the parameters likely to improve stress corrosion cracking resistance. The study was based on the proposition that the resistance to stress corrosion cracking develops from the bridges in the crack wake [17]. The frequency of bridge formation depends on the probability of the crack tip encountering a grain boundary triple junction with a resistant grain boundary (i.e. a non-sensitised boundary). These are boundaries with a high degree of coincidence between the crystal lattice orientations of the grains on either side of the boundary, defined using the coincidence site lattice (CSL) model [18]. Twin boundaries (Σ3) and low CSL

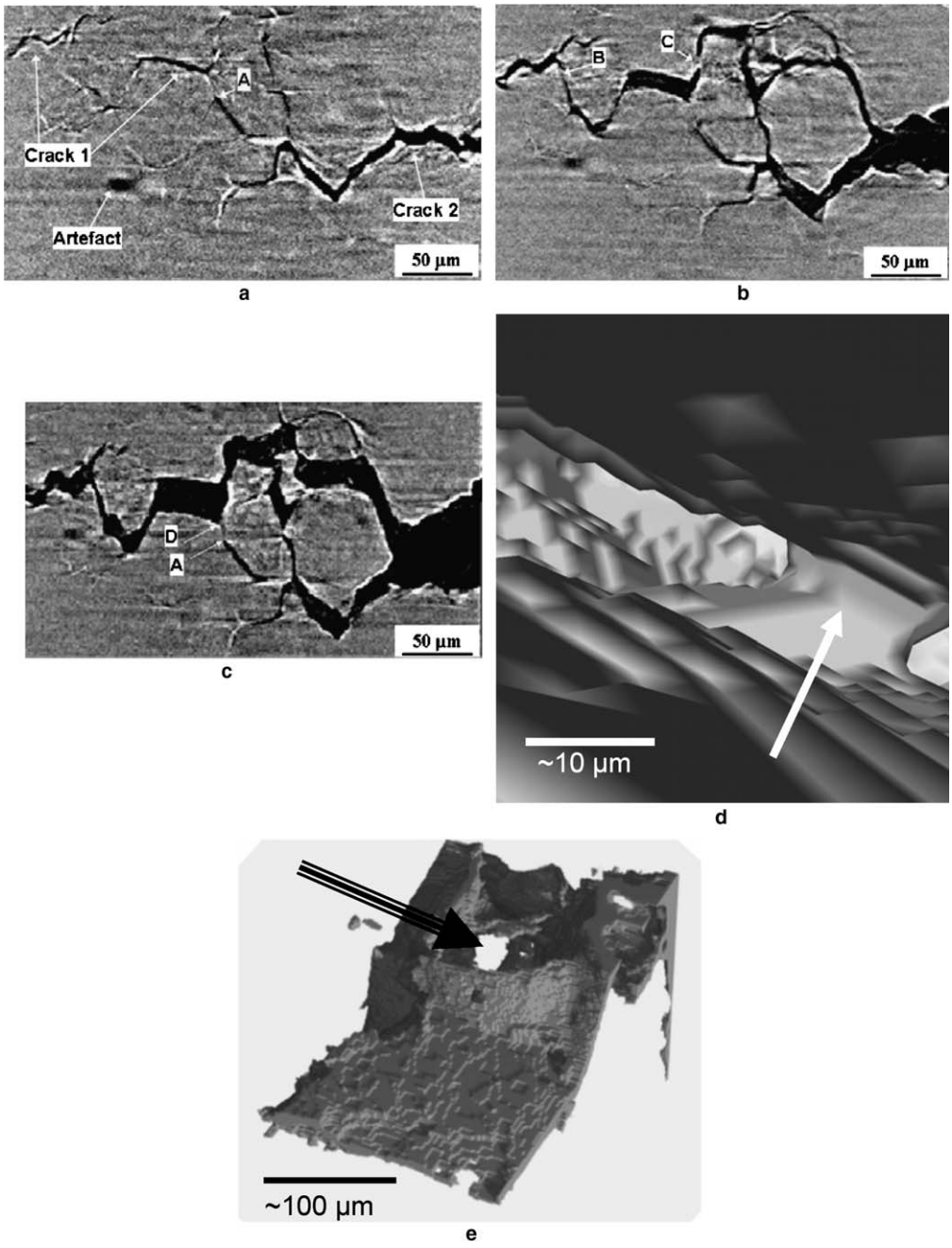


Fig. 2. Tomography data from in situ stress corrosion cracking experiments (pH 2 tetrathionate solution, sensitised 302 stainless steel). (a)–(c) reconstructed longitudinal slices (*yz* plane) of the same region of interest at three different stages in the stress corrosion test, (d) viewed from within the crack, of a crack bridging ligament (indicated by an arrow) and (e) 3D iso-surface rendering of a region of the stress corrosion crack. A 'hole' in the crack, due to the non-fracture of a grain boundary to form a crack bridging ligament is indicated.

boundaries with $\Sigma \leqslant 29$ are commonly regarded as resistant to intergranular corrosion and stress corrosion cracking [5–8]. Crack propagation may also be impeded locally by an unfavourably oriented sensitised boundary. Various percolation-like models [26–29] have been proposed, in which crack arrest is assumed to occur once the crack encounters a resistant feature. The maximum likely crack length,

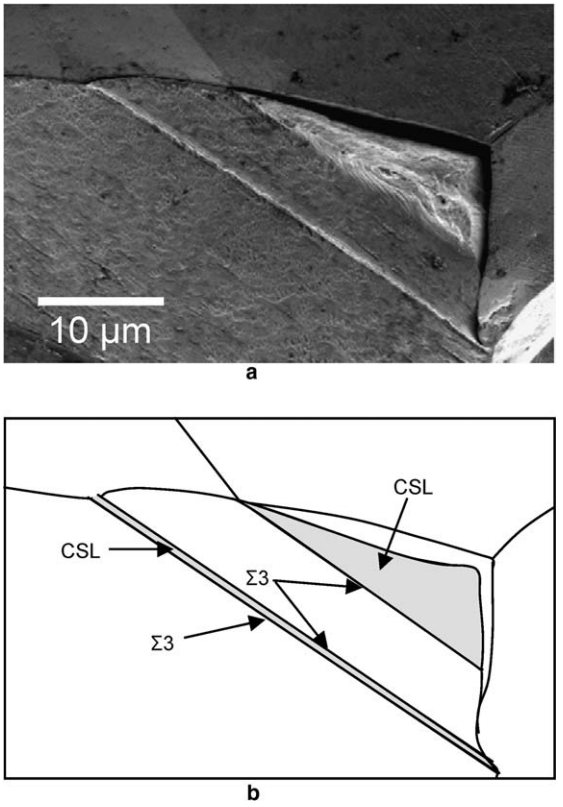


Fig. 3. (a) An example of ductile ligaments, observed on intergranular facets from the fractograph of the failed wire, (b) schematic of the grain shown in (a) with Σ3 twin grain boundaries normal to the page forming a triangular corner twin and a lamella twin. The shaded regions, which correspond to the ductile regions in (a) are postulated to be low CSL segments of the grain boundary formed by the twin growth.

independent of stress, is thus determined by the distribution of resistant triple junctions or grain boundaries.

Our observation of ductile ligaments shows that crack arrest does not necessarily occur when a resistant boundary is encountered. However, the probability of crack bridge formation at a triple junction ($P$) may be expressed in a similar manner to the percolation-like models, using functions such as Eq. (1). Here, $f_{TJ(n-CSL)}$ is the frequency of occurrence of triple junctions with n resistant boundaries (i.e. non-sensitised low CSL, $\Sigma \leqslant 29$) and $f_a$ and $f_b$ are geometrical factors (assumed to be 1 and 0.5 respectively), to account for unfavourably oriented sensitised boundaries at the triple junction. The ratio of $f_{TJ(1-CSL)}$ to $f_{TJ(2-CSL)}$ does not vary significantly over a wide range of microstructures [16], thus the actual values of $f_a$ and $f_b$ are not critical in the relative ranking of microstructures. It is also recognised

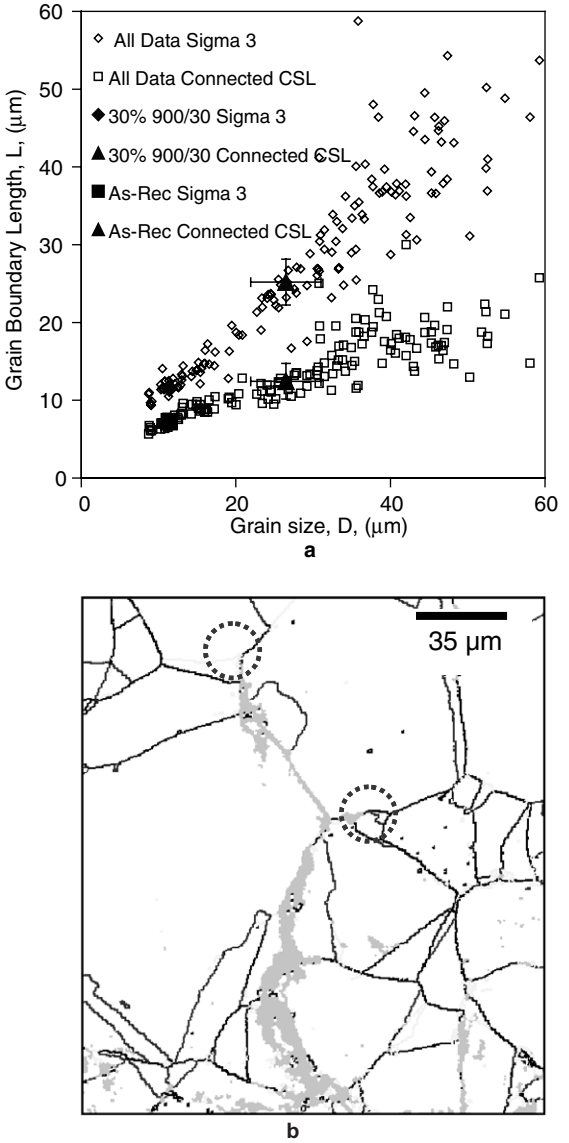


Fig. 4. (a) Effect of grain size on twin length and connected low CSL boundary length in a range of thermo-mechanically processed microstructures (30% strain, annealed at 1173 K–1373 K (900 °C–1100 °C) for 2 min to 24 h). Data for the as-received and 900/30 microstructures are highlighted and (b) EBSD map of a metallographic section of a stress corrosion crack in the as-received microstructure (pH 2.5 tetrathionate solution, sensitised 304 stainless steel). Local crack arrests at 1-CSL and 2-CSL triple junctions are circled. The crack is shown in grey, the twin and CSL boundaries in pale grey, and the high angle grain boundaries in black.

that 2-CSL junctions associated with narrow twins may be characterised as 1-CSL junctions by EBSD. The factor $P$ thus expresses the ratio of the number of triple junctions with potential to form crack

bridges to the total number available to the crack tip.

$$P = \frac{(f_a f_{TJ(2-CSL)} + f_b f_{TJ(1-CSL)})}{1 - f_{TJ(3-CSL)}}. \quad (1)$$

For a one-dimensional model, the probability, $X$, that the crack tip will encounter a resistant triple junction within distance $L$ can be expressed as Eq. (2) [28]. The distance, over which there is a critical probability of bridge formation, say $L_{99\%}$ for $X = 99\%$, will be related to the average distance between crack bridging ligaments on the fracture surface. Since there is a probability that bridging does not occur for a short stress corrosion crack nucleated at a surface until the crack length exceeds $L_{99\%}$, the average crack bridging stress, $\sigma_b$ , will vary with length ($a$) for short cracks. This variation of bridging stress with crack length may have a form such as Eq. (3), such that the average bridging stress depends on the fraction of the crack length ($L$) over which bridging is likely to occur. The crack bridging stress therefore rises and saturates to a maximum value over a length scale determined by $L_{99\%}$, which is a function of both the triple junction distribution (i.e. $P$) and the average distance ($D$) between triple junctions (i.e. grain size). The crack bridging stress acts to shield the crack tip from the applied stress.

$$X = 1 - (1 - P)^{2L/D}, \quad (2)$$

$$\sigma_b = \frac{a - L_{99\%}}{a}$$

$$\sigma_{b\,max} \quad \text{for } a > L_{99\%}, \quad \sigma_b = 0 \quad \text{for } a \leqslant L_{99\%}. \quad (3)$$

The magnitude of the crack bridging stress induced by the ligaments is difficult to determine using a simple model, since with increasing crack opening displacement relative to the ligament size, the ligaments may deform elastically, plastically or rupture. A constant maximum crack bridging stress, $\sigma_{b\,max}$, is currently assumed for all microstructures. If this is sufficient to arrest or significantly retard crack propagation, then microstructures with the greatest resistance to short stress corrosion crack propagation are predicted to be those in which the bridging stress develops more rapidly with crack length. Such microstructures will have smaller grain size and higher $P$ factors. The model described above is closely related to percolation-like models for intergranular stress corrosion cracking, in terms of the relative effects of microstructure parameters. However, it removes the implicit assumption in such models that crack arrest occurs when a resistant junction is encountered. This clearly does not occur due to the three-dimensional nature of the microstructure, as demonstrated by the 3D observations of crack bridging ligament formation. The new model includes the effects of applied stress magnitude, and can be applied to short cracks in residual stress gradients to consider the effects of surface preparation and damage on stress corrosion cracking.

The effect of the bridging stress can be represented using a simple linear elastic fracture mechanics model. The magnitude of crack tip shielding available from bridging ligaments is quite low for short cracks and there is an implicit assumption that stress corrosion cracking occurs with very low values of crack tip strain [30]. Crack propagation occurs if the net crack tip stress intensity factor is greater than a short crack threshold $K_{ISCC}$, which is assumed to be small ($\sim$0.1 MPa$\sqrt{m}$) [17]. The critical threshold stress, $\sigma_{th}$, can then be calculated as the remote applied stress necessary to increase the net crack tip stress intensity factor above $K_{ISCC}$ (Eq. (4)). The variation of threshold stress with crack length is illustrated in Fig. 5 for two different

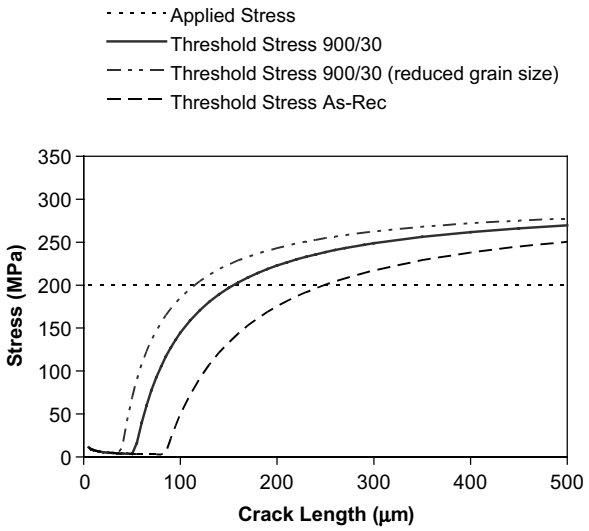


Fig. 5. Predicted development of crack propagation threshold stress with increasing crack length for the 30%/900/30 and as-received test microstructures, compared with an applied stress of 200 MPa. The 30%/900/30 microstructure was cold worked by 30% and annealed at 1173 K (900 °C) for 30 min. The effect of accounting for the expected 30% overestimate in the grain size of the 30%900/30 microstructure is also shown (900/30 reduced grain size). The maximum crack bridging stress has been taken to be 300 MPa for both microstructures. The behaviour at very short crack lengths (<30 μm) is an artefact of the simple linear elastic fracture mechanics model, which is not considered to be valid for crack lengths of the order of 1–2 grain diameters.

microstructures. A semicircular crack, radius $a$, is assumed.

$$\sigma_{th} = \frac{\sqrt{2\pi}(K_{sh} + K_{ISCC})}{\sqrt{a}} \text{ where}$$
$$K_{sh} = \sigma_b \sqrt{a/2\pi}. \quad (4)$$

The model parameters for the two test microstructures (before and after a 30% strain followed by a 30 min anneal at 1173 K (900 °C)) are summarised in Table 3. These two microstructures have quite similar $P$ factors, but differ significantly in grain size. All data was obtained using a constant EBSD sampling step size of 5 μm. This large step size was selected to obtain consistent data over a wide range of microstructures, and measurements using smaller step sizes (>1 μm) have shown that although the number of triple junctions is affected by the step size, the factor $P$ is insensitive to step size. However, the grain size was found to be overestimated when the step size was larger than 20% of the grain size [16]. This is consistent with EBSD observations in other microstructures [31], from which the measured grain size of the 900/30 microstructure is thus expected to be an overestimate, by approximately 30%, relative to the as-received grain size.

In order to assess the effect of microstructure engineering on crack growth, crack propagation tests were performed on the two test microstructures using the double-beam-bent specimen geometry described in the experimental section. Typical crack growth results after 144 h at 200 MPa are given in Fig. 6 for the microstructure processed at 1173 K (900 °C) and annealed for 30 min (900/30), compared to the as-received microstructure. When considering the results it is important to note that X-ray diffraction (XRD) analysis demonstrated that the surface residual stresses introduced by sample preparation were not significant, having a magnitude of less than 50 MPa. The applied stress was also monitored during the tests using XRD, and stress relaxation was not observed. The effects of test duration and test reproducibility were also investigated. The crack populations were stable in each microstructure, demonstrating that measurable crack propagation has ceased within the duration of the test. Further details of these tests for materials having a range of microstructures are described elsewhere [16].

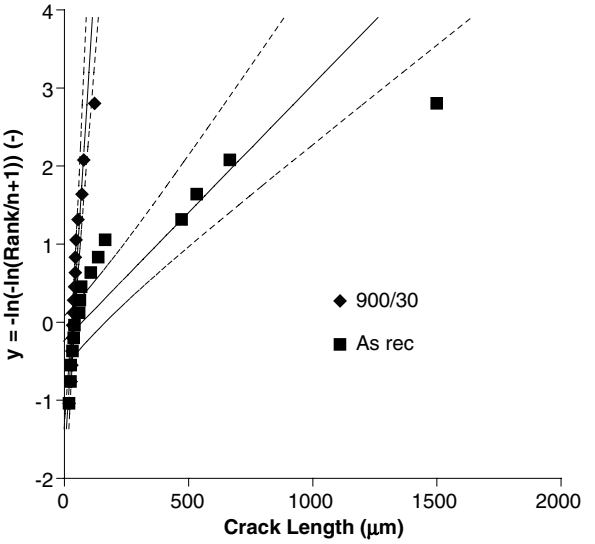


Fig. 6. Crack population data, expressed as the reduced variant ($y$) as a function of the observed crack length for the 30%/900/30 and as-received microstructure tested under an applied stress of 200 MPa for 144 h. The 30%/900/30 microstructure was cold worked by 30% and annealed at 1173 K (900 °C) for 30 min. Solid lines are least square best fits to the data. Dashed lines are the 95% confidence limits.

Simple inspection of the data summarised in Fig. 6 shows that the 900/30 microstructure has the greater resistance to stress corrosion cracking, developing a population of significantly shorter cracks than the as-received microstructure. The parameter $y$, which is derived from the rank of the crack size in the ordered series of $n$ observations

Table 3
Summary of microstructure model parameters for grain boundary and triple junction distribution for the as-received microstructure and after 30% strain, 1173 K (900 °C) annealed for 30 min (900/30)

| Structure | $P$ | Triple junction distribution (%) | | | | $L_{99\%}$ |
|---|---|---|---|---|---|---|
| | | $f_{(0-CSL)}$ | $f_{(1-CSL)}$ | $f_{(2-CSL)}$ | $f_{(3-CSL)}$ | |
| As-rec | 0.43 ± 0.01 | 27.8 ± 1.7 | 52.4 ± 1.0 | 13.8 ± 1.1 | 5.9 ± 3.1 | 84.4 ± 12.7 |
| 900/30 | 0.34 ± 0.01 | 43.0 ± 1.0 | 43.8 ± 1.0 | 11.6 ± 0.8 | 1.6 ± 0.3 | 52.6 ± 1.1 |

Average and range calculated from three measurements. The parameter $L_{99\%}$ was determined from the grain size (including twins) (Table 2).

[21], describes the probability of occurrence of a crack of a given size. This provides a convenient method of describing the population of observed cracks, with comparisons in the maximum likely crack length in the test specimen being made at equivalent values of $y$. The observed difference in maximum crack size is consistent with the relative rates of development of crack bridging predicted for the two microstructures, as defined by the difference in $L_{99\%}$ (Table 3). The predicted variation of threshold stress with crack length is given in Fig. 5, assuming a maximum crack bridging stress of 300 MPa in both microstructures. The proposed model therefore appears reasonable, although it predicts a less significant difference between the two microstructures than is observed. This may be attributed in part to the overestimate in the grain size of the 900/30 microstructure. The predicted effect of reducing the measured grain size by 30% is shown in Fig. 5. Non-random connectivity of susceptible boundaries may also be a factor. The data for the as-received microstructure also does not fit the extreme value distribution well. This indicates that there may be two populations of cracks present. This might be explained by loss of significance of the crack bridging mechanism at longer crack lengths as the crack opening displacements increase.

Current work aims to investigate the crack propagation behaviour in a range of microstructures to determine whether the maximum crack bridging stress is affected by significant variations in $P$. The effects of non-random connectivity of susceptible boundaries and near-surface residual stresses are also being investigated.

## 5. High temperature crack propagation behaviour

Intergranular stress corrosion cracking is a problem in pressurised water cooling systems operating at high temperature. Crack initiation was found to be very difficult in 0.01 M $Na_2SO_4$ electrolyte at 523 K (250 °C) in short times under static load. However intergranular stress corrosion cracking did propagate under autoclave conditions after an

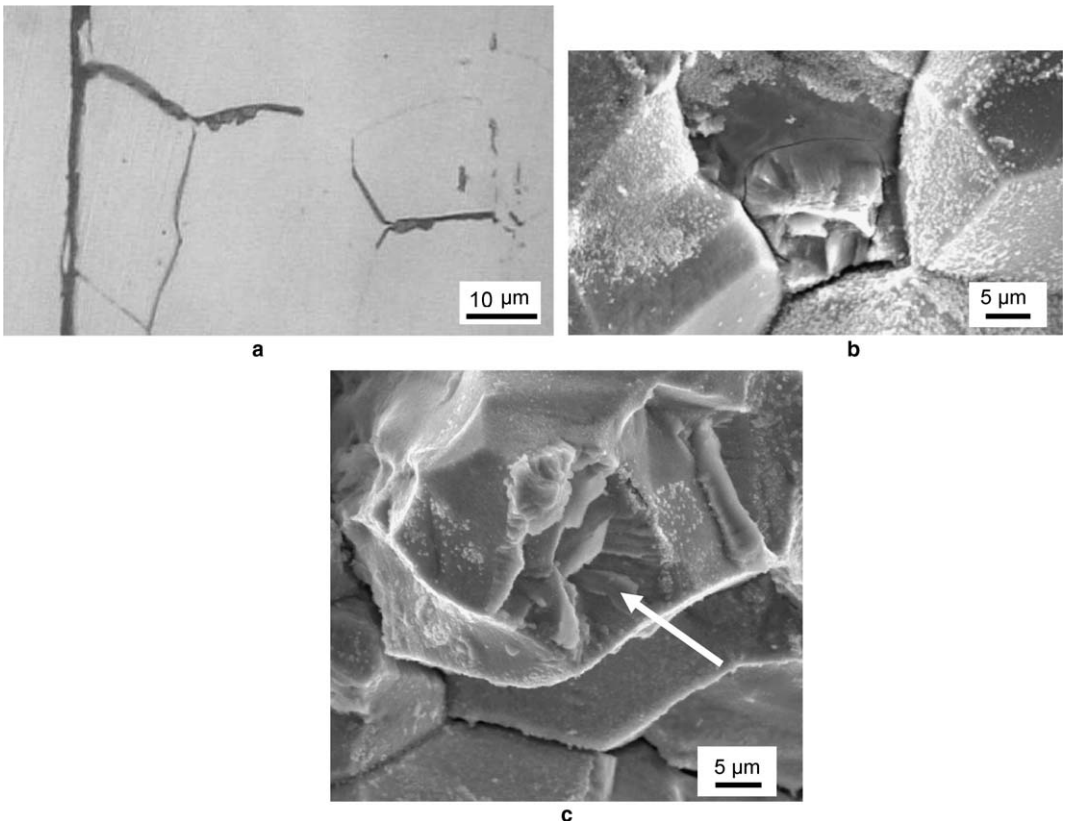


Fig. 7. Crack propagation in the high temperature autoclave environment: (a) metallographic section of intergranular stress corrosion crack (propagating from left to right), (b) ductile ligament on intergranular fracture surface and (c) transgranular cracking (indicated with arrow).

initial exposure of electropolished samples to tetrathionate solution (pH 2.5) for 4 h at room temperature to initiate intergranular corrosion damage at the surface (Fig. 7(a)). The high temperature fracture surface was similar to the room temperature behaviour, with ductile ligament formation (Fig. 7(b)). There was also evidence for some transgranular cracking (Fig. 7(c)). Crack bridging therefore occurs, and microstructure engineering has potential to influence stress corrosion cracking resistance.

The effects of test duration on the depth of stress corrosion crack (SCC) penetration and the depth of the intergranular corrosion damage (IGC) are shown in Fig. 8 for the as-received microstructure. The extreme value distribution for the crack population has been determined.

The data in Fig. 8 shows that the maximum depth of intergranular corrosion, which initiated cracking, is not affected by test duration, whereas the maximum depth of stress corrosion cracking increases with time. This data also suggests that some shorter stress corrosion cracks and intergranular corrosion damage are not clearly distinguished, and there is thus some overlap of the two measured populations. These preliminary results demonstrate that crack propagation rates for short stress corrosion cracks can be determined from these static tests. Measurements of the effects of test duration and stress on the crack population can therefore be employed to investigate the effects of microstructure engineering on stress corrosion crack propagation resistance.

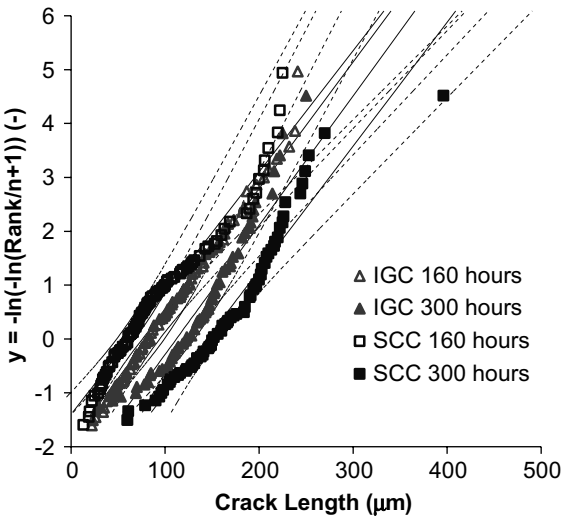


Fig. 8. Effects of test duration on the observed populations of stress corrosion cracking (SCC) and intergranular corrosion damage (IGC) in high temperature autoclave tests in as-received, fully sensitised 304 stainless steel. Solid lines are least square best fits to the data. Dashed lines are the 95% confidence limits.

Work is in progress to investigate the effects of microstructure in this environment, and to confirm whether transgranular cracking in the autoclave environment is associated with the plastically strained crack bridging ligaments. This would have a potentially detrimental effect on the crack shielding mechanism and stress corrosion cracking resistance.

## 6. Three dimensional modelling of crack propagation

While simple models of crack propagation such as that given above provide important insights into stress corrosion cracking, the observation of ductile ligaments due to crack bridging, and the demonstrable effects of microstructure engineering on crack propagation behaviour provide a mechanistic basis for 2D and 3D models for intergranular crack propagation. The aim is to provide a tool for theoretical investigations of the interaction between multiple cracks and the influence of residual stress gradients. Such a model will also provide a better understanding of the elastic/plastic behaviour of crack bridging ligaments and their effect on the crack shielding stresses. A simple 2D model for intergranular crack percolation with crack bridging has been developed, and is described elsewhere [32]. The 3D model is described briefly below. In its present form, the model does not consider the kinetics of crack growth.

At the physical level, the geometry of the microstructure can be represented by a regular tessellation of space into identical cells. As in previous works on percolation modelling of three dimensional intergranular cracking, e.g. [26–29,33,34], the unit cell is chosen to be a truncated octahedron, known also as tetrakaidecahedron or mecon. This is a polyhedron having six square and eight regular hexagonal faces (Fig. 9). The unit cell diameter, $D$, is the edge of the cell bounding cube. This may be considered as a measure of the average grain size. The faces common to neighbouring cells represent grain boundaries, which are classified as either resistant or sensitive to intergranular fracture.

Susceptible boundaries are assumed to fail at a very small strain, $\varepsilon_f$, and without significant inelastic deformations in their vicinity, when encountered by a propagating crack. Resistant boundaries are

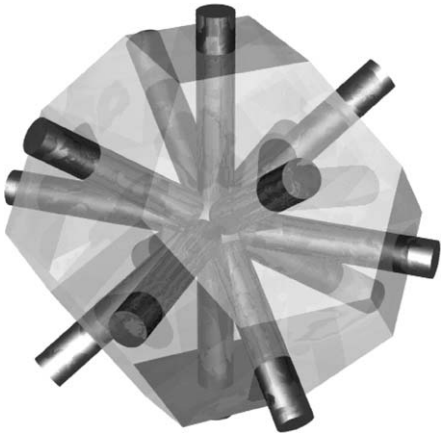

Fig. 9. Physical model of a grain (mecon) for the three-dimensional polycrystalline model and its discrete counterpart using beams.

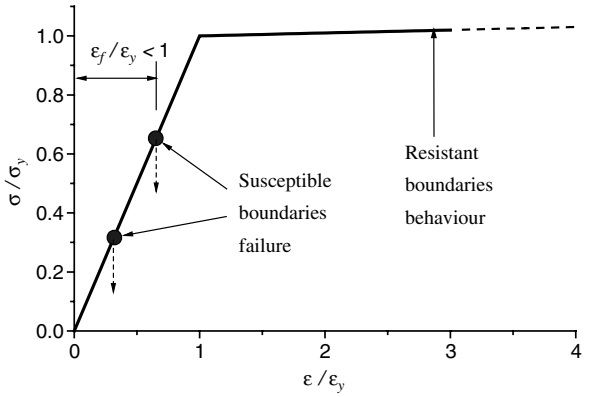


Fig. 10. Schematic illustration of behaviour of susceptible and resistant boundaries employed in the three-dimensional model.

assumed to fail in a ductile mode after a significant amount of accumulated inelastic strain. These properties are consistent with the observed failure mechanisms (e.g. Figs. 2 and 3).

At the computational level, a discrete representation of the assembly of mecons is employed. This is done in view of the subsequent finite element formulation of the crack propagation problem. In the discrete representation, each mecon is substituted by a node at its central point and the mecon's fourteen faces are substituted by beam elements linking it to the central points of the neighbouring mecons. This is shown schematically in Fig. 9, where cylinders represent the beam elements. This leads to a significant reduction of the nodes and elements in a model and hence of the computational effort, which is crucial for three dimensional problems. The element cross sections were varied to ensure that the assembly behaved like a solid under the same deformation when subjected to tensile deformation in the elastic range.

The modelled assembly contains 30 000 grains, which form 198 310 internal grain boundaries (modelled by 30 000 nodes and 198 310 beam elements) in the finite element model. A small intergranular pre-crack is introduced by removing three beam elements. The elements are assumed be elastic–plastic with linear isotropic hardening. Properties typical of an annealed austenitic stainless steel were selected, where relevant, although no attempt has been made to relate the model behaviour to experiment. The modulus of elasticity $E = 200$ GPa and Poisson's ratio $\nu = 0.3$. In the current formulation, the resistant elements have a yield stress $\sigma_y = 200$ MPa with yield strain $\varepsilon_y = 10^{-3}$ and ultimate strength $\sigma_u = 400$ MPa at ultimate strain $\varepsilon_u = 0.1$. Elements representing susceptible boundaries are assumed to fail at strain $\varepsilon_f < \varepsilon_y$ (Fig. 10). The two types of behaviour are randomly distributed among the elements, depending on a given fraction of resistant boundaries, $f$. The load is symmetric and applied via prescribed displacements which introduces a homogeneous strain in the assembly $\varepsilon_\infty = 5 \times 10^{-4}$, equivalent to a homogeneous remotely applied stress $\sigma_\infty \approx 0.5\sigma_y$.

The modelling of crack propagation is handled by two separate software components. Equilibrium is found using the commercial finite element program ABAQUS [35]. The solution is then analysed by a program developed in-house, which examines all elements in contact with the crack surface. Element conditions are compared against their failure criteria, and at most one boundary, being either susceptible or resistant, is allowed to fail per step. Equilibrium is then re-established using ABAQUS, and the analysis is repeated until crack propagation ceases or the simulation is terminated.

Simulations have been performed for different fractions of resistant boundaries. Fig. 11 illustrates the crack configuration after 200 steps of growth, i.e. approximately 200 failed boundaries, in a material with 30% resistant boundaries. A number of crack bridges are clearly identified along the crack surface. This demonstrates the ability of the model to simulate 3D crack propagation.

Current work in progress aims to quantify the effects of crack bridging on the crack shielding in the 3D model, and to study the effects of residual

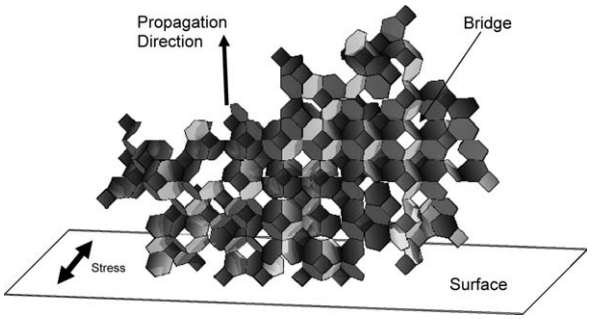


Fig. 11. Three-dimensional crack generated after 200 crack growth steps, showing bridges. The fraction of resistant boundaries was 30%. Only the cracked boundaries are shown – some bridging ligaments are evident as 'holes' in the crack.

stress gradients and crack interactions. Further refinement of the model using experimental results will be necessary before it becomes a useful predictive tool.

## 7. Summary

- Observations of intergranular stress corrosion cracking in sensitised stainless steel show that resistant grain boundaries can bring about crack bridging. It is proposed that these bridges provide resistance to the propagation of short stress corrosion cracks. The development of these bridges and thereby this resistance is affected by the grain boundary triple junction distribution and the grain size.
- This proposition is supported by experimental data for the effect of microstructure engineering on crack propagation resistance. The level of resistance provided by this mechanism may vary with the environment. Transgranular cracking may occur in high temperature/pressure conditions for example.
- The observations provide a mechanistic basis for a new three-dimensional computational model of short stress corrosion crack propagation. Preliminary results demonstrate that the 3D model captures experimentally observed behaviour.

## Acknowledgements

We would like to thank J.-Y. Buffiere and E. Maire of INSA, Lyon for the use of the in situ loading stage and P. Cloetens for help on ID19 at the ESRF. P.J.W. acknowledges support of a Royal Society-Wolfson Merit Award. The support of RR plc for D.E., P.W. and A.P.J. is gratefully acknowledged, as the support of TJM and NS by BNFL through their Materials Performance Centre, a University Research Alliance.

## References

[1] P.M. Scott, Corrosion 56 (2000) 771.
[2] R.C. Newman, Corrosion 57 (2001) 1030.
[3] M. Akashi, G. Nakayama, in: Proceeding of the 9th International Conference on Environmental Degradation of Materials in Nuclear Power Systems, Minerals, Metals & Materials Soc., Warrendale, PA, 1999, p. 389.
[4] T.K. Christman, Corrosion 46 (1990) 450.
[5] S.H. Kim, U. Erb, K.T. Aust, G. Palumbo, Scripta Mater. 44 (2001) 835.
[6] G. Palumbo, K.T. Aust, Can. Metall. Q 34 (1995) 165.
[7] H. Kokawa, M. Shimada, Y.S. Sato, J. Min. Met. Mater. Soc. 52 (2000) 34.
[8] V.Y. Gertsman, S.M. Bruemmer, Acta Mater. 49 (2001) 1589.
[9] S. Ahmad, M.L. Mehta, S.K. Karaf, I.P. Saraswat, Corrosion 38 (1982) 347.
[10] H.H. Horowitz, Corros. Sci. 23 (1983) 353.
[11] B.W. Bennett, H.W. Pickering, Metall. Trans. 18A (1987) 1117.
[12] W. Ludwig, J.Y. Buffiere, S. Savelli, P. Cloetens, Acta Mater. 51 (2003) 585.
[13] J. Baruchel, P. Cloetens, J. Hartwig, W. Ludwig, L. Mancini, P. Pernot, M. Schlenker, J. Synch. Rad. 7 (2000) 196.
[14] J. Marrow, P.J. Withers, J.Y. Buffiere, R.C. Newman, D. Engelberg, L. Babout, G. Johnson, ESRF Experimental Report: ME577, 2003. Available from: <http://ftp.esrf.fr/pub/UserReports/25143_A.pdf>.
[15] T.J. Marrow, L. Babout, B.J. Connolly, D. Engelberg, G. Johnson, J.Y. Buffiere, P.J. Withers, R.C. Newman, Environment-Induced Cracking of Metals (EICM-2), Banff, Canada, 2004.
[16] D. Engelberg, PhD thesis, Grain Boundary Engineering for Intergranular Stress Corrosion Resistance in Austenitic Stainless Steel, University of Manchester, 2005.
[17] D. Engelberg, T.J. Marrow, R.C. Newman, L. Babout, Environment-Induced Cracking of Metals (EICM-2), Banff, Canada, 2004.
[18] H. Grimmer, W. Bollmann, D.H. Warrington, Acta Cryst. A30 (1974) 197.
[19] D.G. Brandon, Acta Metall. 14 (1966) 1479.
[20] ASTM G-39: Standard Practice for Preparation and Use of Bent-Beam Stress-Corrosion Test Specimens, 1999.
[21] E.J. Gumbel, Statistics of Extremes, Columbia University, 1958.
[22] M. Kokawa, Introduction to Life Prediction of Industrial Plant Materials – Application of Extreme Value Statistical Method for Corrosion Analysis, Allerton, 1994.
[23] J. Marrow, V. Luprano, S. Roberts, J. Am. Ceram. Soc. 76 (1993) 2915.
[24] R.J. Young, J. Microsc. 185 (1997) 199.
[25] Mercury Computer Systems, 2004. Available from: <http://www.amiravis.com>.

[26] E.M. Lehockey, G. Palumbo, P. Lin, A.M. Brennenstuhl, Scripta Mater. 36 (1997) 1211.
[27] G. Palumbo, P.J. King, K.T. Aust, U. Erb, P.C. Lichtenberger, Scripta Metall. Mater. 25 (1991) 1775.
[28] V.Y. Gertsman, K. Tangri, R.Z. Valiev, Acta Metall. Mater. 42 (1994) 1785.
[29] E.M. Lehockey, A.M. Brennenstuhl, I. Thompson, Corros. Sci. 46 (2004) 2383.
[30] L.E. Thomas, S.M. Bruemmer, Corrosion 56 (2000) 572.
[31] F.J. Humphreys, J. Mater. Sci. 36 (2001) 3833.
[32] A.P. Jivkov, N.P.C. Stevens, T.J. Marrow, First International Conference on the Simulation of Electrochemical Processes (ElectroCor 05), Cadiz, Spain, 2005.
[33] L.C. Lim, T. Watanabe, Acta Metall. Mater. 38 (1990) 2507.
[34] A. Garbacz, M.W. Grabski, Acta Metall. Mater. 41 (1993) 469.
[35] ABAQUS User's Manual, Version 6.4, Abaqus Inc., 2004.